Journal of Theoretical Biology 333 (2013) 135–145

Contents lists available at SciVerse ScienceDirect

Journal of Theoretical Biology

journal homepage: www.elsevier.com/locate/yjtbi

A single formula to describe radiation-induced protein relocalization: Towards a mathematical definition of individual radiosensitivity

Larry Bodgi [a,b], Adeline Granzotto [a], Clément Devic [a], Guillaume Vogin [a], Annick Lesne [c], Jean-François Bottollier-Depois [d], Jean-Marc Victor [c], Mira Maalouf [b], Georges Fares [b], Nicolas Foray [a,*]

[a] Institut national de la Santé et de la Recherche Médicale (INSERM), UMR1052—Radiobiology Group, Cancer Research Centre of Lyon, 28 Rue Laennec, 69008, Lyon, France
[b] Université Saint-Joseph, Faculté des sciences, 1107-2050 Beyrouth, Liban
[c] Centre National de la Recherche Scientifique (CNRS), UMR7600, laboratoire de physique théorique de la matière condensée, 75252 Paris, France
[d] Institut national de la Radioprotection et de la Sûreté Nucléaire (IRSN)—DRPH, Service de Dosimétrie Externe, 92260 Fontenay-aux-Roses, France

HIGHLIGHTS

- A number of stress response proteins relocalize in nucleus as identifiable foci.
- We propose a single formula to describe appearance/disappearance kinetics of foci.
- The parameters of the Bodgi's function allows to define radiosensitivity.

ARTICLE INFO

Article history:
Received 30 January 2013
Received in revised form
6 May 2013
Accepted 21 May 2013
Available online 2 June 2013

Keywords:
DNA repair
Immunofluorescence
Radiosensitivity
Radiation

ABSTRACT

Immunofluorescence with antibodies against DNA damage repair and signaling protein is revolutionarising the estimation of the genotoxic risk. Indeed, a number of stress response proteins relocalize in nucleus as identifiable foci whose number, pattern and appearance/disappearance rate depend on several parameters such as the stress nature, dose, time and individual factor. Few authors proposed biomathematical tools to describe them in a unified formula that would be relevant for all the relocalizable proteins. Based on our two previous reports in this Journal (Foray et al., 2005; Gastaldo et al., 2008), we considered that foci response to stress is composed of a recognition and a repair phase, both described by an inverse power function provided from a Euler's Gamma distribution. The resulting unified formula called "Bodgi's function" is able to describe appearance/disappearance kinetics of nuclear foci after any condition of genotoxic stress. By applying the Bodgi's formula to DNA damage repair data from 45 patients treated with radiotherapy, we deduced a classification of human radiosensitivity based on objective molecular criteria, notably like the number of unrepaired DNA double-strand breaks and the radiation-induced nucleo-shuttling of the ATM kinase.

1. Introduction

To date there is increasing evidence that unrepaired DNA damage are responsible for cell lethality and tissue radiosensitivity, and that misrepaired DNA damage are linked to genomic instability and cancer proneness (Jeggo and Lobrich, 2007; Joubert et al., 2008). Immunofluorescence technique that allows the detection of individual DNA damage and protein relocalization via appropriate antibodies is upsetting the estimation of the genotoxic risk, notably that linked to ionizing radiation exposure (Rothkamm and Lobrich, 2003). Indeed, some DNA damage repair and signaling proteins have been shown to relocalize after genotoxic stress as discrete nuclear foci, which facilitates their quantification and provides information about the spatial distribution of the early biophysical events at the origin of DNA damage (Fig. 1). After stress, nuclear foci generally appear and disappear at rates that depend on numerous parameters such as dose, post-stress time and individuals (Bekker-Jensen and Mailand, 2010; Bekker-Jensen et al., 2006; FitzGerald et al., 2009; Franchitto and Pichierri, 2002; Maser et al., 1997; Mirzoeva and Petrini, 2001; Neumaier et al., 2012; Rothkamm and Lobrich, 2003; Scully et al., 1997; Stewart et al., 2003). The quantification of the radiation-induced

* Corresponding author. Tel.: +33 426556794.
E-mail address: Nicolas.foray@inserm.fr (N. Foray).

0022-5193/$ - see front matter © 2013 Elsevier Ltd. All rights reserved.
http://dx.doi.org/10.1016/j.jtbi.2013.05.020

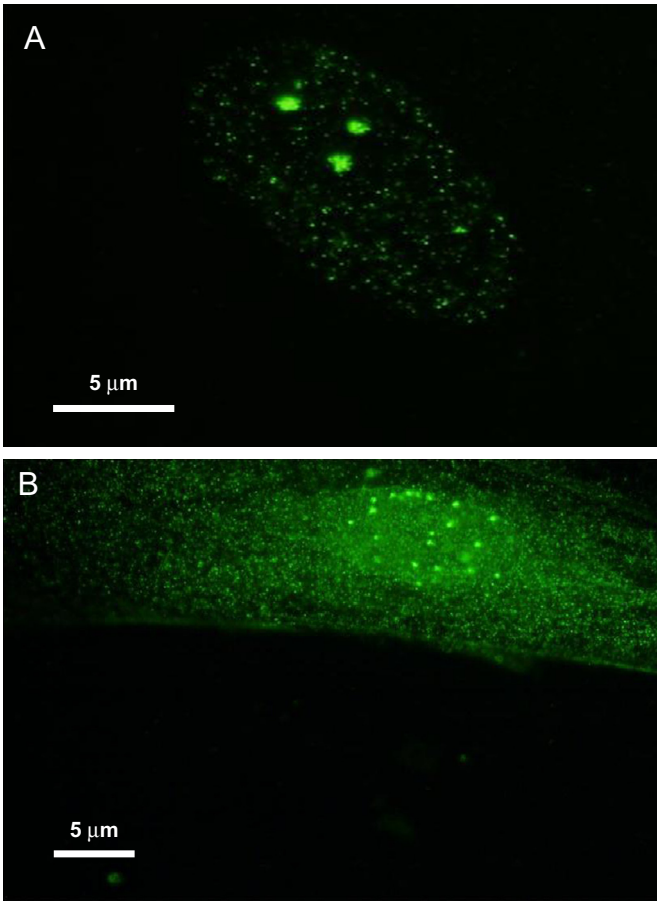

Fig. 1. Representative examples of immunofluorescence images of human fibroblasts labeled by γ-H2AX (A) or pATM (B) antibodies. Nuclear foci are visible in nucleus with both antibodies while cytoplasmic staining is only observed with pATM marker.

nuclear foci is also at the basis of biological dosimetry that may be useful in case of nuclear accident or estimation of the dose after medical exposure response (Jakob and Durante, 2012; Kinner et al., 2008; Testard and Sabatier, 1999).

It was shown that immunofluorescence with antibodies against the phosphorylated forms of the variant H2AX histone (γH2AX) allows the detection of DNA double-strand breaks (DSB), the key-DNA damage of the radiation response (Jakob and Durante, 2012; Kinner et al., 2008; Rothkamm and Lobrich, 2003). The γH2AX foci reflect the radiation-induced DSB that are recognized by the major mammalian DSB repair pathway, the non-homologous end-joining (NHEJ). While γH2AX foci were found to be an interesting biomarker of the radiation response, they present a variety of patterns whose biological significance is not fully understood yet (Costes et al., 2010; Neumaier et al., 2012). Some other proteins like 53BP1, MDC1, MRE11, etc., phosphorylated generally, show radiation-induced relocalization as nuclear foci but with different choreography: appearance in 1 min to some hours, disappearance in some min to several hours (Bekker-Jensen and Mailand, 2010; Bekker-Jensen et al., 2006; FitzGerald et al., 2009; Franchitto and Pichierri, 2002; Maser et al., 1997; Mirzoeva and Petrini, 2001; Neumaier et al., 2012; Rothkamm and Lobrich, 2003; Scully et al., 1997; Stewart et al., 2003) (see also Section 5). Despite the intensive use of immunofluorescence, there are only a few biomathematical studies of the kinetics of appearance/disappearance of nuclear foci (Jakob and Durante, 2012; Kinner et al., 2008; Lisby and Rothstein, 2009; Lisby et al., 2004; Neumaier et al., 2012; Rothkamm and Lobrich, 2003). Unified models describing the nuclear foci choreography would however help in establishing molecular models of radiosensitivity. In two previous papers, we provided evidence that the repair rate of *individual* DNA damage is time-independent whereas *a population* of DNA damage is time-dependent and obeys the Gamma probability distribution (Foray et al., 2005; Gastaldo et al., 2008). Here, we propose a unified formula that describes kinetics of appearance/disappearance of nuclear foci relevant for any protein involved in the major DSB repair and signaling pathways. This model permits to establish temporal correlations between different downstream and upstream actors of radiation response and to quantify the radiosensitivity risk.

2. The model

2.1. Main principles

In response to any DNA breaking agent, DNA damage repair and signaling proteins relocalize as nuclear immunofluorescence foci by generally obeying two kinetic phases:

- *The foci appearance phase:* during which the number of foci increases and reaches its maximum at a rate, value and post-stress time that depend on many parameters like dose and individual factors. Such phase may possibly be preceded by the nucleo-shuttling of some proteins and leads to DNA damage recognition;
- *The foci disappearance phase:* during which the number of foci decreases up to a residual value, at a rate that depends on many parameters like dose and individual factors. The rate of foci disappearance is not necessarily linked to the rate of foci appearance. Such phase is generally interpreted as repair of DNA damage.

Hence, the total number of DNA damage revealed by nuclear foci observed by immunofluorescence, assessed at a given post-stress time t after a single dose D, $N(t,D)$, obeys the following equation:

$$\frac{dN(t)}{dt} = (K_{rec} - K_{rep})N \quad (1)$$

where K_{rec} is the DNA damage recognition rate and K_{rep} is the DNA damage repair rate.

Throughout this model, we considered each DNA damage *taken individually* (*microscopic approach*) and characterized by constant transition rates k. Thereafter, we considered *the DNA damage subpopulations* with time-dependent transition rates K (*macroscopic approach*) (Foray et al., 2005; Gastaldo et al., 2008). We deliberately chose to take DSB induced by X- or gamma-rays as an example. However, our model is relevant for other genotoxic stress and types of DNA damage (data not shown) (Foray et al., 2005; Gastaldo et al., 2008).

2.2. Induction of DSB

The number of DSB physically induced by X-rays (or gamma-rays) assessed immediately after irradiation (*i.e.* without effect of repair), $N_{ind}(D)$, is linearly dose-dependent and is about 40 (37 ± 5) DSB per Gy per human diploid cell in our hands (Foray et al., 1997; Joubert et al., 2008). Hence, in the frame of *microscopic* view, the DSB induction rate k is assumed to be *constant*. In the case of X-rays (or gamma-rays) irradiations that are not targeted (*e.g.* microirradiation), all the cells receive the same dose. Consequently, in the frame of *macroscopic* view, there is a single population of cells with a constant DSB induction rate $K_{ind} = k_{ind}$.

The number of *induced* DSB, $n(k)$, is therefore:

$$n(k) = kD(2a) \tag{2a}$$

$$N_{ind}(D) = K_{ind}D \tag{2b}$$

For X-rays and human diploid cells:

$$k = K_{ind} = 40 \tag{2c}$$

2.3. Recognition of DSB

To be recognized by DNA repair and signaling pathway, DSB is assessed following radiation exposure. Therefore, the number of induced DSB must be included in the definition of the number of recognized DSB. The DSB recognition step also includes eventual nucleo-shuttling of proteins and the period of time required for damage recognition. As specified above, DSB recognition rate is not dependent on DSB repair rate but depends on many physical, chemical and biological factors. The number of recognized DSB does not necessarily increase immediately after irradiation and $N_{rec}(t)$ can appear as a sigmoid function. Hence, as a first step, we described $N_{rec}(t)$ with a logistic (Verhulst) model (Tsoularis and Wallace, 2002; Verhulst, 1838, 1846). In this case, a logistic model integrates the possibility that the recognition rate is limited by the total number of X-rays-induced DSB (N_{max}). In the frame of a logistic model, the recognition rate K of DSB linearly decreases as a function of time t, as follows:

$$K(t) = K(0).\left(1 - \frac{N(t)}{N_{max}}\right) \tag{3a}$$

The total number of recognized DSB, $N(t)$ obeys the following equation:

$$\frac{dN}{dt} = K(0)N(t)\left(1 - \frac{N(t)}{N_{max}}\right) \tag{3b}$$

with

$$N(t) = \frac{N_{max}}{1 + e^{-K(0)(t-t_0)}} \tag{3c}$$

$$N(t_0) = \frac{N_{max}}{2} \tag{3d}$$

However, in practice, DSB recognition function shows a period of latency only for certain radioresistant cells. It may be explained by the presence of a small quantity of proteins in the nucleus already involved in the recognition process *before irradiation* (data not shown). To be also relevant for radiosensitive cells, DSB recognition function should be therefore more hyperbolic than sigmoid. Hence, we chose to replace the logistic model by a curvilinear model.

Any experimental protocol involving radiation is assumed to induce a *specific* and *continuous* spectrum of DSB differing by their own recognition rate k. The k value represents the transition rate per unit of time (min^{-1}) from a *"non-recognized"* to a *"recognized" substate*. In the frame of *microscopic* view, the recognition rate k is assumed to be *constant*, independent of the post-irradiation time. The number of *"non-still recognized"* DSB with a given recognition rate k, $n(t,k)$, varies with post-irradiation time t, as follows:

$$\frac{dn(t,k)}{dt} = -k\, n(t,k) \tag{4a}$$

$$n(t,k) = n(0,k)e^{-kt} \tag{4b}$$

The number of radiation-induced DNA damage is assumed to be so large that each k cannot be assessed individually. In the frame of the *macroscopic* view, the total number *"non-still recognized"* DSB, $N_{nonrec}(t)$, is defined with the recognition rate K of a population of DSB with different k as:

$$\frac{dN_{nonrec}(t)}{dt} = -K_{nonrec}N(t) \tag{5a}$$

By derivating $N_{nonrec}(t)$ from Eq. (4b):

$$\frac{dN(t)}{dt} = -\frac{\int_0^\infty kP(k)e^{-kt}dk}{\int_0^\infty P(k)e^{-kt}dk}N(t) = -K(t)N(t) \tag{5b}$$

In previous papers (Foray et al., 2005; Gastaldo et al., 2008), we already showed that a solution of Eqs. (5a) and (5b) can be an inverse power function $F(t,a,b)$ relevant with the Gamma distribution function, as follows:

$$F(t) = C\left(\frac{1}{1+bt}\right)^a \tag{6a}$$

where a and b are adjustable transition rate parameters, and C is a constant.

Hence,

$$N_{nonrec}(t) = C\left(\frac{1}{1+b_{nonrec}t}\right)^{a_{nonrec}} \tag{6b}$$

If one considers the total number of *"recognized"* DSB, $N_{rec}(t)$, and the corresponding transition rate b_{rec}, $b_{rec}=b_{nonrec}$ and $a_{rec}=a_{nonrec}$. Therefore, at any time t:

$$N_{rec}(t) = N_{ind} - N_{nonrec}(t) \tag{7a}$$

Thus:

$$N_{rec}(t) = C\left(1 - \left(\frac{1}{1+b_{rec}t}\right)^{a_{rec}}\right) \tag{7b}$$

By considering that all induced DSB are recognized:

$$N_{rec}(t) = ID\left(1 - \left(\frac{1}{1+b_{rec}t}\right)^{a_{rec}}\right) \tag{7c}$$

$$K_{rec}(t) = \frac{a_{rec}b_{rec}}{1 + b_{rec}t + (1+b_{rec}t)^{a_{rec}}} \tag{7d}$$

where a_{rec} and b_{rec} are adjustable parameters.

Interestingly, the function $N_{rec}(t)$ in (7b) is a curvilinear function, therefore reaching the requirements for the DSB recognition of human cells specified above.

2.4. Repair of DSB

To be repaired, DSB must be recognized by DNA repair and signaling pathway. Therefore, the number of recognized DSB must be included in the definition of the number of repaired DSB. The description of our DSB repair kinetics model based on both microscopic and macroscopic approaches was published previously (Foray et al., 2005; Gastaldo et al., 2008). Briefly, any experimental protocol involving radiation is assumed to induce a *specific* and *continuous* spectrum of DSB differing by their own repair rate k. The k value represents the transition rate per unit of time (min^{-1}) from a *"non-repaired"* to a *"repaired" substate. The repair rate* k is assumed to be *constant*, independent of the post-irradiation time. The number of DNA damage with a given repair rate k, $n(t,k)$, varies with post-irradiation time t, as follows:

$$\frac{dn(t,k)}{dt} = -k\, n(t,k) \tag{8a}$$

$$n(t,k) = n(0,k)e^{-kt} \tag{8b}$$

The number of radiation-induced DNA damage is assumed to be so large that each k cannot be individually assessed. It has been shown that the total number of DSB at a given repair time t obeys:

$$\frac{dN_{rep}(t)}{dt} = -K_{rep}N(t) \tag{9a}$$

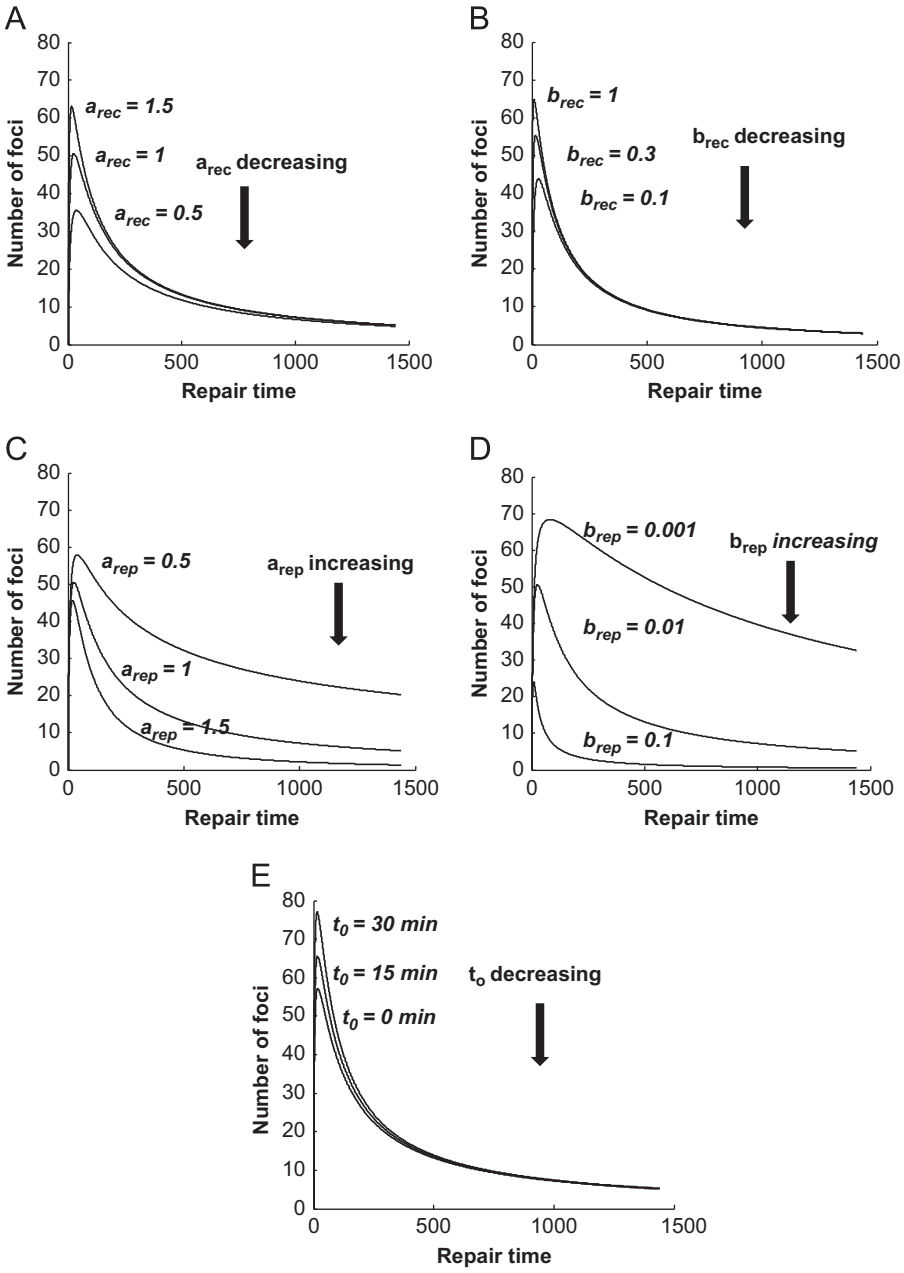

Fig. 2. Shape of the Bodgi's curve and impact of each parameter values: From data fit of γ-H2AX foci data provided from cell lines showing moderate radiosensitivity irradiated at 2 Gy, each parameter value was fixed to the indicated values and the Bodgi's function was generated from 0 to 24 h post-irradiation times.

$$N_{\mathrm{rep}}(t) = C\left(\frac{1}{1+b_{\mathrm{rep}}t}\right)^{a_{\mathrm{rep}}} \tag{9b}$$

where C is a constant.

By considering that all induced DSB are repairable:

$$N_{\mathrm{rep}}(t) = ID\left(\frac{1}{1+b_{\mathrm{rep}}t}\right)^{a_{\mathrm{rep}}} \tag{9c}$$

$$K_{\mathrm{rep}}(t) = \frac{a_{\mathrm{rep}}b_{\mathrm{rep}}}{1+b_{\mathrm{rep}}t} \tag{9d}$$

where a_{rep} and b_{rep} are adjustable parameters.

2.5. The Bodgi's function

The total number of foci observed at any time by immunofluorescence is the result of the competition between processes that make foci appear or disappear. The competition between DNA damage induction, recognition and repair phases is the most frequent situation. We introduced the possibility of a possible delay between the recognition and the repair process. By considering Eqs. (1), (7c) and (9c), the total number of DSB detected by immunofluorescence against a given biomarker, at any post-irradiation time and dose D, N(t,D), becomes:

$$\frac{dN(t,D)}{dt} = (K_{\mathrm{rec}} - K_{\mathrm{rep}})N \tag{1}$$

Thus

$$\mathrm{N(t)} = \mathrm{C}\left(1-\left(\frac{1}{1+\mathrm{b_{rec}t}}\right)^{\mathrm{a_{rec}}}\right)\left(\frac{1}{1+\mathrm{b_{rep}(t-t_0)}}\right)^{\mathrm{a_{rep}}} \tag{10a}$$

where C is a constant.

If we consider that all the induced DSB are recognized, and that repair is negligible (very low b_{rep}), $N(t)$ will tend to the number of induced DSB.

Therefore:

$$N(t) = ID\left(1-\left(\frac{1}{1+b_{rec}t}\right)^{a_{rec}}\right)\left(\frac{1}{1+b_{rep}(t-t_0)}\right)^{a_{rep}} \quad (10b)$$

In which:

- I is the induced number of foci per Gy;
- a_{rec} and b_{rec} are the recognition rate parameters;
- a_{rep} and b_{rep} are the repair rate parameters;
- t_0 represents the delay between the recognition and the repair process.

It is noteworthy that a and b parameters maybe dose-dependent functions.

The authors proposed to call this function the **Bodgi's function** to honor the work quality of the first author. The **Bodgi's function** permits to describe the appearance/disappearance of nuclear foci formed by any protein in response to genotoxic stress.

As first approximation for mammalian cells, when DSB is considered as DNA damage and when repair times exceeds some hours, the Bodgi's function becomes (see also Section 3):

$$N(t) = \frac{ID}{1+b_{rep}(t,D)} \quad (10c)$$

3. Results

3.1. Properties of the Bodgi's function parameters and shape of the curves

The Bodgi's formula is a function of 6 adjustable parameters (we will see below that some parameters are constant or may be neglected in certain conditions). In order to investigate how each parameter influences the shape of the Bodgi's curve, we fixed the induction rate I as constant (40 DSB per Gy per cell; 80 at 2 Gy) for describing X-rays-induced DSB in human cells and successively, a_{rec}, b_{rec}, a_{rep}, b_{rep} and t_0 (Fig. 2). By choosing realistic parameter values, it appeared that:

- The lower a_{rec} or b_{rec}, the slower recognition rate, the lower maximal number of foci. It is noteworthy that the a_{rec} and b_{rec} values act significantly on the shape of the curve for early times (earlier than 2 h post-stress).
- The lower a_{rep} or b_{rep} the slower repair rate, the higher number of residual damage. It is noteworthy that a_{rep} and b_{rep} values act significantly on the shape of the curve for long times (later than 4 h post-stress).
- The lower t_0, the lower maximal number of foci.

In practice, we observed that a_{rec} was systematically found to be equal to 1 for DSB data in human cells (data not shown).

3.2. Quality of data fit with the Bodgi's function

It is noteworthy that the choice of investigated repair times (10 min, 1, 4, 24 h) was justified by ancillary DSB repair data from more than 100 human cell lines that cover the widest range of human radiosensitivity (Foray et al., 1997; Joubert et al., 2008). Experimental foci data show a significant variability due to the multiparametric nature of the biological response to stress, experimental protocol and incompressible 5% relative error. Since the number of foci decreases with repair time, the lowest number of foci to be scored and, thus, the lowest absolute error of foci scoring are generally observed for 24 h data. Furthermore, the short interval between 0 and 10 min post-irradiation times artificially impacts on the weight of the 10 min data by comparison with the other repair times chosen.

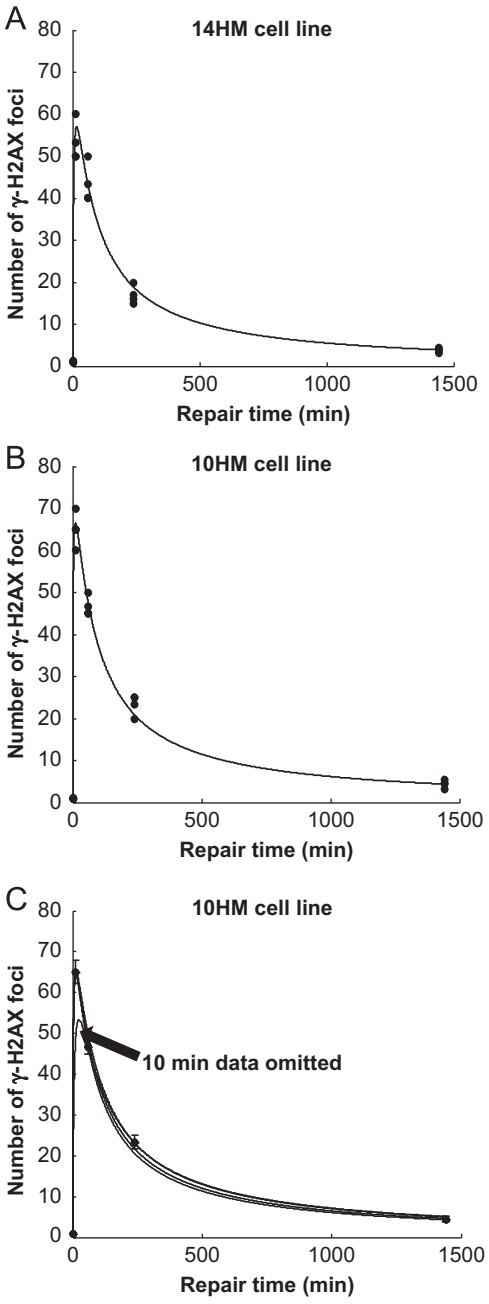

Fig. 3. Robustness of the Bodgi's curve and impact of the number of data plot: γ-H2AX foci data provided from two cell lines provided from representative radiosensitive patients (12HM (A) and 12HM (B)) irradiated at 2 Gy were fitted to the Bodgi's curve. Table 1 presents the parameter values of fits performed on separated or pooled replicated experiments. Here is represented the fit obtained from the pooled data. Each data plot from each experiment is represented. By omitting 10 min, 1h, 4 h or else 24 h plot, 10 HM data were fitted again. Curves represented the result of the corresponding fits.

We evaluated the robustness of the Bodgi's function between 10 min and 24 h post-irradiation (Fig. 3). As a first step, γ–H2AX data from 3 independent replicates taken separately were fitted. As a second step, we fitted the average values of the 3 replicates (Fig. 3). Table 1 shows the adjustable parameter values for 2 representative human cell lines from radiosensitive patients deduced from separated or pooled experiments. The fit quality was estimated by using the residual least squared (LSQ) (see Section 5). First, it is noteworthy that the Bodgi's function provided

Table 1
Adjustable parameters values of the Bodgi's function after fitting γH2AX data from 2 representative patient cell lines from separated or pooled replicated experiments. The least squared values defined in Section 5 reflect the data fit quality.

Cell line	Experiment	Parameters					LSQ for each experimental data point				
		a_{rec}	b_{rec} (min^{-1})	a_{rep}	b_{rep} (min^{-1})	t_0 (min)	10 min	1 h	4 h	24 h	Mean
10HM	1	1	0.34	1	0.012	7.5	0.00	10	17	1.1	5.7
	2	1	0.58	1	0.010	5.1	0.00	25	3.6	2.1	6.2
	3	1	0.87	1	0.015	8.9	0.27	1.2	6.4	1.6	1.9
	Mean	1	0.59	1	0.012	5.7	0.01	5.7	1.0	1.6	1.7
12HM	1	1	0.50	1	0.010	0.2	0.22	5.9	6.5	0.26	2.6
	2	1	0.25	1	0.015	1.0	0.12	0.04	1.3	0.01	0.30
	3	1	0.26	1	0.015	0.2	0.12	0.16	4.5	0.22	1.0
	Mean	1	0.31	1	0.013	0.2	3.00	0.01	3.7	0	1.3

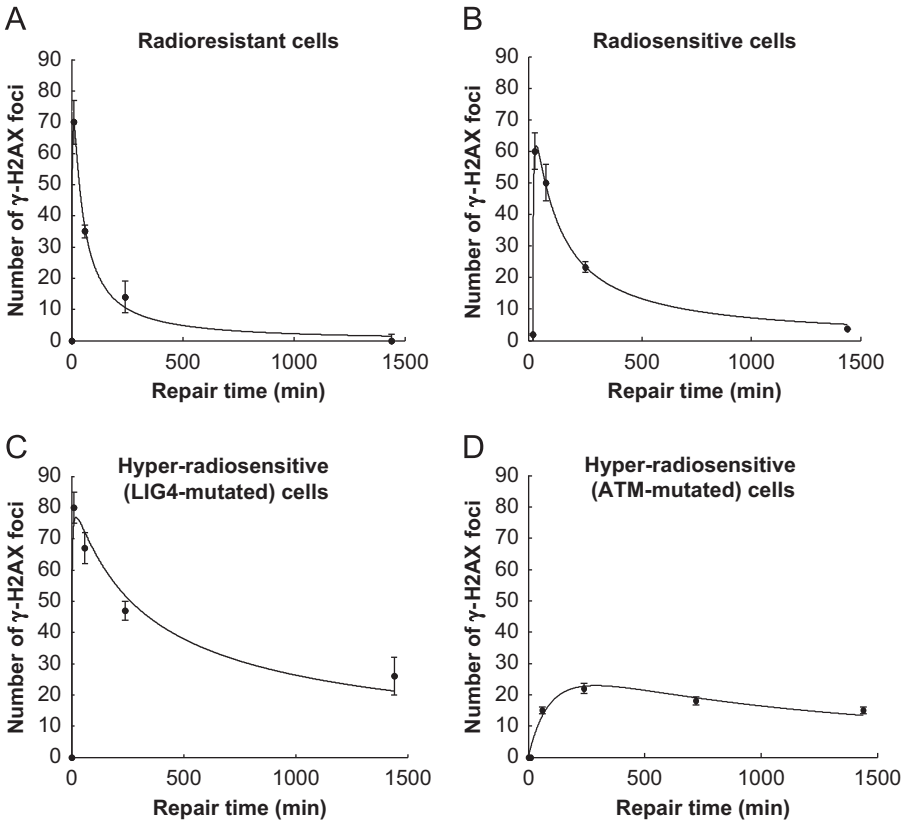

Fig. 4. γH2AX foci data fitted to the Bodgi's function: γ-H2AX foci data from representative cell lines of the collection were fitted to the Bodgi's function. Each data plot represents the mean ± standard error of the mean (SEM) of the 3 replicates. Four situations have been encountered: radioresistant cells (here the GP cell line) (panel A), cells with moderate radiosensitivity (here the 14HM cell line) (panel B), the only case of LIG4-mutation (the 180BR cell line) (panel C) and the hyper-radiosensitive ATM-mutated cells (here the AT5BI cell line) (panel D).

good fits with regard to the poor number of points and the inter-replicated fluctuations. As expected, fluctuations around b_{rep} parameters are reduced since the repair phase covers the 1–24 h post-irradiation times range while recognition phase is defined only by the value of the 10 min data plot. Consequently, t_0 value can vary up to 50% according to the number of data to be fitted (Fig. 3). The variation of the a_{rec}, b_{rec}, a_{rep}, b_{rep} and t_0 parameters values should be compensated by getting more repair time plots. However, the acquisition of the 4 repair times data for a given kinetics already represents an important experimental effort inasmuch as the collection used here is made of 45 cell lines, one of the largest investigated. As a second step, we omitted one data plot (10 min, 1, 4, or else 24 h) and re-fitted data and calculated the corresponding LSQ. It appeared that the omission of 10 min plot only significantly affects the shape of the curve as shown in Fig. 3C. This observation may be explained by the general rapidity of the DSB recognition process that conditions 2 among 5 parameters whereas 2 data points in the 1–24 h repair time range among the 3 chosen are sufficient for a good fit of the DSB repair phase (Fig. 3).

3.3. *Inter-individual differences of γ–H2AX and ATM foci kinetics*

In response to DSB inducers, the ATM protein kinase is known to auto-phosphorylate (pATM forms) and to phosphorylate H2AX (*γ–H2AX*) (Foray et al., 2003; Guo et al., 2010). The pATM forms proceed to a nucleo-shutlling from cytoplasm to nucleus and relocalize as discrete foci (Krueger et al., 2007; Yang et al., 2011). As DNA scaffold constituents, the γ–H2AX forms are systematically visible as nuclear foci at the DSB recognition sites. By using our

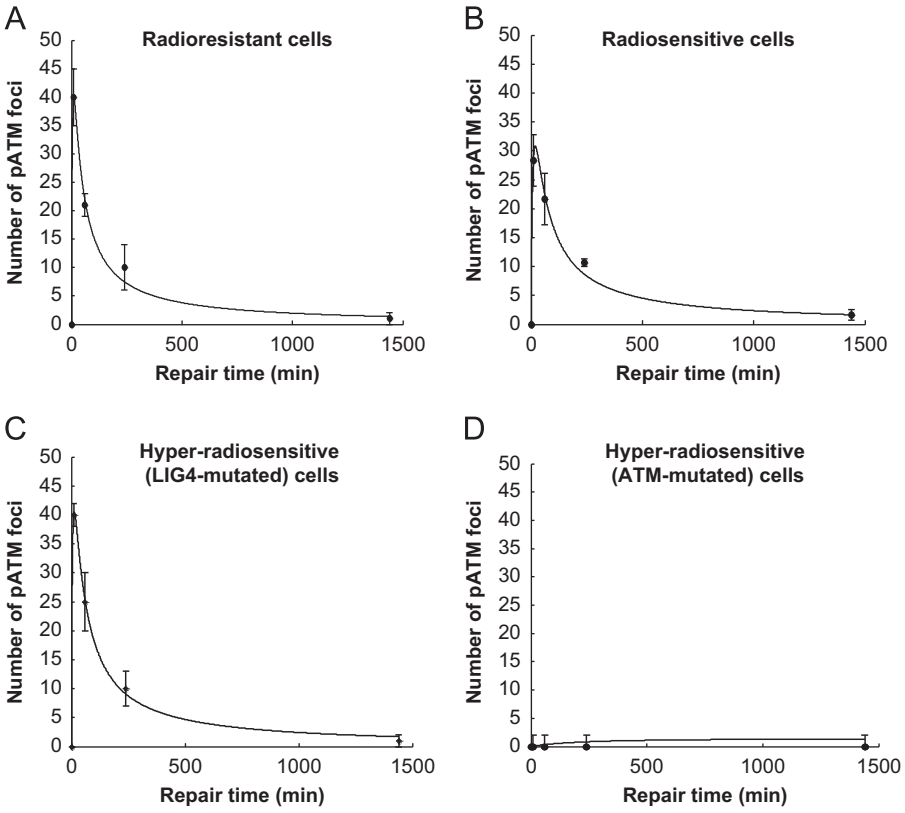

Fig. 5. pATM foci data fitted to the Bodgi's function: pATM foci data from representative cell lines of the collection were fitted to the Bodgi's function. Each data plot represents the mean ± standard error of the mean (SEM) of the 3 replicates. Four situations have been encountered: radioresistant cells (here the GP cell line) (panel A), cells with moderate radiosensitivity (here the 14HM cell line) (panel B), the only case of LIG4-mutation (the 180BR cell line) (panel C) and the hyper-radiosensitive ATM-mutated cells (here the AT5BI cell line) in which pATM is absent (panel D).

Table 2
Ranges of the parameters values from the fit of γ–H2AX and pATM data from the 45 fibroblast cell lines of the collection.

Parameter	γ-H2AX			pATM		
	Group I	Group II	Group III	Group I	Group II	Group II
a_{rec}	1	1	1	1	1	1
b_{rec}	[0.3, 0.6]	[0.01, 1]	[0.001, 1]	[0.1, 0.3]	[0.005, 0.1]	[0.001, 0.3]
a_{rep}	1.2	1	[0.7, 1]	1	1	1
b_{rep}	[0.02, 0.03]	[0.005, 0.015]	[0.001, 0.005]	[0.03, 0.05]	[0.005, 0.03]	[0.001, 0.4]
t_0	[10. 15]	[0, 50]	[0, 30]	0	0	0

collection of 45 human fibroblasts provided from patients treated with radiotherapy, we fitted the γ–H2AX and pATM foci data to the Bodgi's function (Figs. 4 and 5). Our model provided good fits for all the data and each series of a_{rec}, b_{rec}, a_{rep}, b_{rep} and t_0 parameters defines one single cell line. Table 2 shows the ranges of each parameter value. Interestingly, while patients suffer from different radiosensitivity, it appeared that some groups of cells elicited some parameters values in common. We examined therefore the relationship between each parameter and each biomarker:

- a_{rec}(γ-H2AX) and a_{rec}(pATM) were found to be equal to 1 for the majority of cell lines and fixed thereafter to this value
- a_{rep}(γ-H2AX) was found to range between 0.7 and 1.2. We deliberately chosen not to fix it during data fitting. Furthermore, a_{rep}(pATM) was found to be equal to 1 and fixed thereafter.
- there is no significant correlation between b_{rec} and b_{rep} and t_0 for a given biomarker (γ-H2AX or else pATM) or for both biomarkers (*e.g.* b_{rec}(γ-H2AX) *vs.* b_{rep}(pATM)), which justifies the data fitting by keeping these both parameters free.
- t_0(γ-H2AX) was found to range from 0 to 36 min and t_0 (pATM) was found to be equal to 0 and was fixed thereafter (Table 2).

Since autophosphorylation and nucleo-shuttling of pATM are events upstream (earlier than) the γ-H2AX foci formation, pATM foci formation likely reflects the time range of DNA damage recognition process. Conversely, the γ-H2AX foci appearance and disappearance was correlated with the DSB repair process (Joubert et al., 2008). Interestingly, when b_{rep}(γ-H2AX) values were plotted against b_{rec}(pATM) values, cell lines were more discriminated than with any other combination of parameter (Fig. 6). Hence, by considering all the 45 cell lines of the collection:

- the b_{rep}(γ–H2AX) range can define 3 distinct groups of radiosensitivity (I, II and III)
- the b_{rec}(pATM) range can define 2 rates of pATM nucleo-shuttling (subgroups *a* and *b*)

Group I corresponds to the radioresistant cells with b_{rep}(γ–H2AX) higher than 0.02 min^{-1} (corresponding to a DSB repair half-time lower than 50 min) and b_{rec} (pATM) higher than

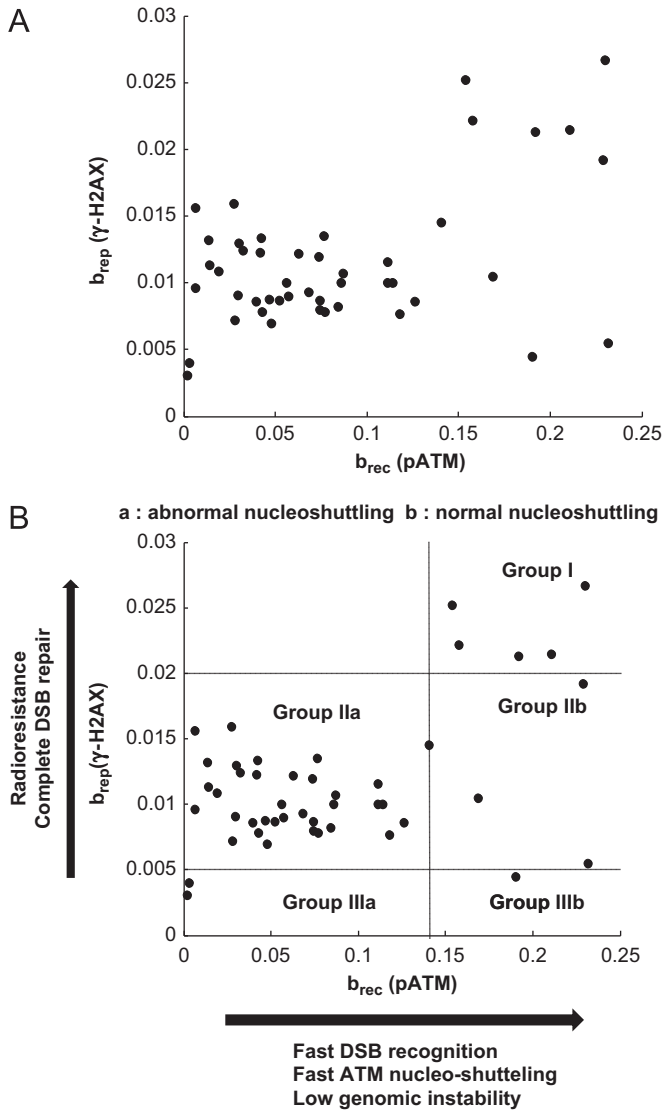

Fig. 6. Quantitative definition of the radiosensitivity groups from Bodgi's function parameters: A: $b_{rep}(\gamma H2AX)$ values from data provided by the 45 cell lines of the collection were plotted against $b_{rec}(pATM)$ values. B: Similar data shown in panel B but with definitions of the groups and subgroups of radiosensitivity.

Table 3
Ranges of the parameters values for ATM/ATR phosphorylation substrates.

Protein	a_{rec}	b_{rec}	a_{rep}	b_{rep}	t_o
NBS1	1	0.075	1	0.010	0
pATR	1	0.045	1	0.065	0
53BP1	1	0.037	1	0.011	0
BRCA1	1	0.0075	1	0.006	0
MRE11	1	0.0034	1	0.005	0

0.14 min^{-1} (corresponding to a DSB recognition half-time lower than 7 min).

Group II corresponds to the cells of patients showing moderate radiosensitivity and cancer proneness with $b_{rep}(\gamma$–H2AX) ranging from 0.005 to 0.02 min^{-1} (corresponding to a DSB repair half-time ranging 50 min to 3 h). The values of b_{rec}(pATM) define subgroups *a* and *b* with slower and normal pATM nucleo-shuttling, respectively.

Group III corresponds to the cells of patients showing hyper-radiosensitivity and cancer proneness with $b_{rep}(\gamma$–H2AX) lower 0.005 min^{-1} (corresponding to a DSB repair half-time longer than 3 h). The values of b_{rep}(pATM) define subgroups *a* and *b* with slower (like ATM-mutated cells) or normal pATM nucleo-shuttling (like LIG4-mutated cells), respectively (Fig. 6).

3.4. Relevance of the Bodgi's function to describe foci kinetics for any protein

To examine whether the Bodgi's function allows good fit of foci data from other proteins than γ-H2AX and pATM, we performed immunofluorescence on a radioresistant cell line irradiated with antibodies against ATM phosphorylation substrates like NBS1, 53BP1, ATR, MRE11, BRCA1. Table 3 shows the fitting parameters values. The Bodgi's function provided good quality of fits for all the proteins tested and parameters values (notably b_{rec} and b_{rec}) may be useful to propose a temporal hierarchy between foci formation of all these proteins (Foray et al., 2003).

4. Discussion

4.1. Kinetics of nuclear foci appearance/disappearance: a complex cascade of phosphorylations

To date, immunofluorescence technique is upsetting our approach of quantification of genotoxic stress by allowing the detection of individual DNA damage inside each cell. As a consequence, there is a plethora of recent studies involving various softwares for nuclear foci scoring that consider the shape, size, granulometry and fluorescence intensity of foci (Costes et al., 2006, 2010; Lisby et al., 2004; Neumaier et al., 2012; Rothkamm and Lobrich, 2003). Surprisingly, while mathematical models may be useful for a better understanding of molecular and cellular mechanisms of stress response, few reports, if any, aimed to describe kinetics of foci appearance/disappearance independently of the nature of the foci-inducer proteins. In fact, in addition to the complexity of the molecular process involved, this relative absence of a model unifying both DNA damage recognition and repair phases can be explained by uncertainties around general paradigms for describing stress response since the biological role of some stress actor is still misknown. It must particularly be stressed that the nucleo-shuttling of ATM is still poorly studied since it is still widely considered that the nuclear forms are the only active ones (Krueger et al., 2007; Yang et al., 2011). However, even if ATM kinase and nuclear DSB repair protein are fully active, impairment and/or delay in the nucleo-shuttling of pATM forms may also result in unrepairable DSB and radiosensitivity as in a number of genetic syndromes.

Proteins that relocalize as nuclear foci after stress are generally kinases themselves or phosphorylated substrates of kinases that may be nuclear but also cytoplasmic. It has been shown that genotoxic stress activates ATM and ATR kinases which successively phosphorylate specific substrates in a temporal and conditional hierarchy (Foray et al., 2003). In the first seconds to minutes post-stress, proteins involved in DNA damage recognition are activated. First, they are generally DNA binding proteins, already in the nucleus like histone H2AX (Rothkamm et al., 2003). Thereafter, proteins involved in DNA repair *per se* are activated (Foray et al., 2003). However, the majority of them are so abundant in the nucleus that they do not form nuclear foci like Ku80, Ku70 and ligase 4. There are some counterexamples like foci formed by Rad52 and Rad51 but these proteins generally relocalize in S-G2-M rather than in G0/G1 (Bekker-Jensen and Mailand, 2010; Bekker-Jensen et al., 2006). Proteins that control cell cycle checkpoints elicit nuclear foci between a few minutes to a few hours after

irradiation like BRCA1, BRCA2, pCHK2 whose forms may be nuclear but also cytoplasmic (Foray et al., 2003; Scully et al., 1997). Finally, proteins involved in cellular death pathways like the phosphorylation forms of c-jun protein that specifically trigger apoptosis, relocalize in nucleus but generally not as discrete foci. Hence, proteins forming foci are notably ATM/ATR subtrates that are phosphorylated mostly between the DNA damage recognition and the next cycle checkpoint (Foray et al., 2003).

The molecular response to ionizing radiation is a representative example of a cascade of successive phosphorylations that range from the very first second to some several hours after exposure. However, the rapidity and the extent of this phenomenon are necessarily limited by the number of DNA damage *i.e.* strongly dependent on the dose. Hence, a_{rec}, b_{rec}, a_{rep}, b_{rep} parameters must be considered as functions of the dose in a more general approach, as mentioned in the Model Chapter. Besides, it is noteworthy that a_{rec}, b_{rec}, a_{rep}, b_{rep} are not necessarily linear functions of the dose. Firstly, the kinetics of ATM nucleo-shuttling should depend on the degree of oxidization induced by radiation that may be itself not linearly dose-dependent. Secondly, one Gy X-rays acutely produces 10,000 base damage (BD), 1000 single-strand breaks (SSB) and 40 DSB per human diploid cell, whatever the genetic status of the cell (Granzotto et al., 2011). Although base damage are the most rapidly repairable DNA damage, abnormal repair of base damage may result in the formation of additional SSB, and similarly, abnormal repair of SSB may result in the formation of additional DSB. Hence, during the repair course, it is not surprising to observe maximal activity a few minutes after the end of the stress exposure that does not obey a linear function of the dose (Granzotto et al., 2011). In addition to the dose-impact on the kinetics of foci appearance/disappearance, the number of foci should depend on the pools of functional protein. Hence, while DNA damage produced by biologically relevant radiation doses (*i.e.* medical exposures) are generally less numerous than protein molecules, active proteins may be unavailable in the nucleus immediately after stress. The diversity of all these situations led us to validate our model with cells from a large number of patients showing a large range of radiosensitivity. The Bodgi's function has therefore the advantage to describe a complex biological phenomenon in a unified model.

4.2. Justifications of the choices for the model

As specified above, the kinetics of foci appearance/disappearance may be described in 2 phases that biostatistical models should take into account: DNA damage recognition, and DNA damage repair phases. With regard to the repair phase, the description of the repair kinetic was widely discussed in our previous reports (Foray et al., 1996, 1998, 2005; Gastaldo et al., 2008). Notably, it appears clear that DNA damage repair kinetic do not simply result from Michealis–Menten approach and that Eulers's gamma distribution is more relevant for describing DNA damage than Poisson or Gauss distributions (Foray et al., 2005; Sutherland, 2006). From these conclusions, the formula (9c) was validated for different types of DNA damage and stress (Gastaldo et al., 2008). The formula (9c), an inverse power function of time and dose does not immediately evoke a common biostatistical situation in radiation biology but the microscopic and macroscopic approaches help us to better understand the final complexity of the repair transition rate $K_{rep}(t)$. The obvious multiproteic nature of DNA damage repair process that involves several proteins and substrates on a period of time ranging from minutes to several hours suggests to us a possible re-formulation of the function (9c) in terms of fluctuations around successive steps of DNA damage repair (Fig. 6). Further investigations are however needed to reach this aim.

With regard to the recognition phase, it appeared convenient to consider firstly that the non-recognized DNA damage obey also the same formula, and therefore formula (7c) was deduced. Lastly, to take into account the eventual period of times: (1) between the beginning of nucleo-shuttling and the recognition of DNA damage; (2) between the recognition of DNA damage and the beginning of DNA repair, the parameter t_0 was therefore required. With regard to the recognition phase, DNA damage sensoring is hypothesized to be the result of a stress-induced oxydo-reduction that oxidizes ATM proteins and facilitate their progressive nucleo-shuttling (Guo et al., 2010). The DNA damage recognition therefore resembles a diffusion process throughout the nuclear membranes with a certain velocity that obeys a hyperbolic law (Fig. 6). Similar processes can be observed in electricity with accumulator. Hence, new evolutions of the Bodgi's function may introduce a diffusion-like coefficient that may describe more adequately the process of ATM nucleo-shuttling.

4.3. Towards a quantitative definition of the radiosensitivity risk

Interestingly, our double approach (microscopic view and macroscopic view) was very useful to distinguish the fate of an individual DNA damage, an individual cell or a population of cells. In fact, it must be stressed that in each cell, there is a competition between NHEJ and recombination repair pathways (Joubert et al., 2008; Lobrich and Jeggo, 2005). Hence, throughout the data fit from different biomarkers, the Bodgi's function allows the description of the functionality of these two DSB repair pathways and therefore is very useful for the estimation of the risk of toxicity and genomic instability. As a result, it appears obvious that the Bodgi's function describes any level of human radiosensitivity and unpublished data revealed also the robustness for other cell lines of rodent origin (data not shown). By showing that the molecular response to radiation of a number of patients may be discriminated by DSB recognition via b_{rec}(pATM) values or else by DSB repair via a_{rep}(γH2AX) values, we were able to distinguish what patient suffers from a delay in the ATM nucleo-shuttling (subgroup a) or else from a DSB repair deficiency *per se* (subgroups b). Interestingly, it appears that group II patients from subgroup a show a less marked radiosensitivity than patients showing DSB repair impairments, confirming that DSB repair is a crucial step of the radiation response. On another hand, group I patients, characterized by a low cancer proneness and a strong radioresistance elicit generally normal ATM nucleo-shuttling, suggesting that a delay in DSB recognition may favor misrepair of DSB that will be not managed by NHEJ. Conversely, the majority of group II patients show cancer proneness and a minority of them shows a strong radiosensitivity.

Since the a and b parameters are dependent on the dose, the Bodgi's function can be used whatever the radiation dose to the condition that the functions a_{rec}(D), b_{rec}(D) a_{rep}(D), b_{rep}(D) were known. Hence, the Bodgi's function may be at the origin of the determination of the molecular basis of radiosensitivity that is generally described by the linear-quadratic clonogenic survival curve $S(D)=\exp(-\alpha D-\beta D^2)$ where α and β are two empirical and adjustable parameters. This paper may serve to express these α and β parameters as a function of DSB repair. This will be the next step of our investigations.

5. Materials and methods

5.1. Cell lines

Untransformed primary fibroblasts used in this study were provided from skin biopsy from patients treated with radiotherapy

performed in non-irradiated area by following national ethical procedures and updated regulations. The details of this collection will be found elsewhere. ATM and LIG4-mutated fibroblasts were added to the collection in order to better define radiosensitivity group III (see details in (Foray et al., 1997; Joubert et al., 2008)). Cell culture has been routinely performed in the lab by following standards detailed elsewhere (Foray et al., 1997; Joubert et al., 2008).

5.2. Irradiation

Irradiations were performed at the anti-cancer centre Léon-Bérard (Lyon, France) on a SL15 medical accelerator (Elekta, Crawley, UK) that delivers 6 MV photons with certified dosimetry at at dose-rate of 3 Gy min^{-1}. Cells were irradiated (2 Gy) at a confluence (3-days plateau phase) in Petri dishes. Immediately after irradiation, cells were incubated at 37 °C for the indicated times.

5.3. Immunofluorescence

The immunofluorescence protocol employed was described elsewhere (Foray et al., 2003). Briefly, cells were fixed in 3% paraformaldehyde 2% sucrose PBS for 15 min at room temperature and permeabilized in 20 mM HEPES, pH 7.4, 50 mM NaCl, 3 mM $MgCl_2$, 300 mM sucrose 0.5% Triton X-100 (Sigma-Aldrich, L'Isle d'Abeau-Chesne, France) for 3 min. Thereafter, coverslips were washed in PBS prior to immunostaining. Primary antibody incubations were performed for 40 min at 37 °C in PBS supplemented with 2% bovine serum fraction V albumin (BSA) (Sigma-Aldrich) and followed by PBS washing. To the exception of anti-$pH2AX^{ser139}$ (1:800), primary antibodies were used at 1:100. Anti-$pH2AX^{ser139}$ antibodies were provided by Upstate Biotechnology-Euromedex (Mundolsheim, France). Anti-*MRE11* antibodies were purchased from Abcys (Paris, France). Anti-$pATM^{ser1981}$ (Clone 10H11.E12; #05-740) and Anti-53BP1 (clone BP18) were produced by Millipore (Molsheim, France). Anti-BRCA1(Ab-1) antibodies were purchased from Oncogene Research (Darmstag, Germany). Anti-pATR (ab 2905) was purchased from ABCAM (Paris, France). Anti-NBS1 was purchased from Novus (Cambridge, UK). Incubations with anti-mouse FITC or with anti-rabbit TRITC secondary antibodies (1:100; Sigma-Aldrich) were performed at 37 °C in 2% BSA for 20 min. Coverslips were mounted in Vectashield containing 4,6-Diamidino-2-phenylindole (DAPI) (Abcys, Paris, France) to counterstain the nuclei. Coverslips were examined with an Olympus fluorescence microscope. DAPI-staining permitted also to indirectly evaluate yield of G_1 cells (nuclei with homogeneous DAPI staining), S cells (nuclei showing numerous pH2AX foci), G_2 cells (nuclei with heterogeneous DAPI staining) and metaphase (visible chromosomes). In order to avoid any bias by using imaging analysis software, the number of foci per cell was determined after eye-scoring in about 50 cells in G0/G1 per slide. The reliability of such analysis was controlled by the accumulation of a number of raw data (Joubert et al., 2008).

5.4. Data fit

The data fit was obtained by minimizing the least squares residual R^2. The algorithm used was the trust-region-reflective optimization which is based on the interior-reflective Newton method (Coleman and Li, 1996). The least squares calculations were obtained by using the lsqcurvefit command in Matlab Software (The Mathwork, Natick, MA, USA), and were stopped when the final change in the sum of squares relative to its initial value became less than the default value of the function tolerance.

Acknowledgments

We thank Madame Beaufrère for her assistance in editing English. L.B. was supported by the Association pour l'Ataxie Telangiectasie (APRAT), Université Saint-Joseph and Mount Lebanon Hospital (Beirut, Lebanon), CMIRA Rhône-Alpes Region Grant and the French-Lebanese CEDRE and EIFFEL project (French and Lebanese Ambassies). This work was also supported by the Association Pour la Recherche sur l'Ataxie-Telangiectasie (APRAT), the Electricité de France (Comité de Radioprotection), the Plan Cancer/AVIESAN "Micromegas project, the ANR "Hemi-breaks T" project and the Centre National d'Etudes Spatiales (CNES).

References

Bekker-Jensen, S., Mailand, N., 2010. Assembly and function of DNA double-strand break repair foci in mammalian cells. DNA Repair (Amst) 9, 1219–1228.
Bekker-Jensen, S., Lukas, C., Kitagawa, R., Melander, F., Kastan, M.B., Bartek, J., Lukas, J., 2006. Spatial organization of the mammalian genome surveillance machinery in response to DNA strand breaks. J. Cell Biol. 173, 195–206.
Coleman, T.F., Li, Y., 1996. An interior, trust region approach for nonlinear minimization subject to bounds. SIAM J. Optim. 6, 418–445.
Costes, S.V., Chiolo, I., Pluth, J.M., Barcellos-Hoff, M.H., Jakob, B., 2010. Spatiotemporal characterization of ionizing radiation induced DNA damage foci and their relation to chromatin organization. Mutat. Res. 704, 78–87.
Costes, S.V., Boissiere, A., Ravani, S., Romano, R., Parvin, B., Barcellos-Hoff, M.H., 2006. Imaging features that discriminate between foci induced by high- and low-LET radiation in human fibroblasts. Radiat. Res. 165, 505–515.
FitzGerald, J.E., Grenon, M., Lowndes, N.F., 2009. 53BP1: function and mechanisms of focal recruitment. Biochem. Soc. Trans. 37, 897–904.
Foray, N., Badie, C., Alsbeih, G., Fertil, B., Malaise, E.P., 1996. A new model describing the curves for repair of both DNA double-strand breaks and chromosome damage. Radiat. Res. 146, 53–60.
Foray, N., Charvet, A.M., Duchemin, D., Favaudon, V., Lavalette, D., 2005. The repair rate of radiation-induced DNA damage: a stochastic interpretation based on the gamma function. J. Theor. Biol. 236, 448–458.
Foray, N., Priestley, A., Alsbeih, G., Badie, C., Capulas, E.P., Arlett, C.F., Malaise, E.P., 1997. Hypersensitivity of ataxia telangiectasia fibroblasts to ionizing radiation is associated with a repair deficiency of DNA double-strand breaks. Int. J. Radiat. Biol. 72, 271–283.
Foray, N., Monroco, C., Marples, B., Hendry, J.H., Fertil, B., Goodhead, D.T., Arlett, C.F., Malaise, E.P., 1998. Repair of radiation-induced DNA double-strand breaks in human fibroblasts is consistent with a continuous spectrum of repair probability. Int. J. Radiat. Biol. 74, 551–560.
Foray, N., Marot, D., Gabriel, A., Randrianarison, V., Carr, A.M., Perricaudet, M., Ashworth, A., Jeggo, P., 2003. A subset of ATM- and ATR-dependent phosphorylation events requires the BRCA1 protein. Embo. J. 22, 2860–2871.
Franchitto, A., Pichierri, P., 2002. Bloom's syndrome protein is required for correct relocalization of RAD50/MRE11/NBS1 complex after replication fork arrest. J. Cell Biol. 157, 19–30.
Gastaldo, J., Viau, M., Bouchot, M., Joubert, A., Charvet, A.M., Foray, N., 2008. Induction and repair rate of DNA damage: a unified model for describing effects of external and internal irradiation and contamination with heavy metals. J. Theor. Biol. 251, 68–81.
Granzotto, A., Joubert, A., Viau, M., Devic, C., Maalouf, M., Thomas, C., Vogin, G., Malek, K., Colin, C., Balosso, J., Foray, N., 2011. Individual response to ionising radiation: what predictive assay(s) to choose? Comptes Rendus de l'Académie des Sciences 334, 140–157.
Guo, Z., Kozlov, S., Lavin, M.F., Person, M.D., Paull, T.T., 2010. ATM activation by oxidative stress. Science 330, 517–521.
Jakob, B., Durante, M., 2012. Radiation dose detection by imaging response in biological targets. Radiat. Res. 177, 524–532.
Jeggo, P.A., Lobrich, M., 2007. DNA double-strand breaks: their cellular and clinical impact? Oncogene 26, 7717–7719.
Joubert, A., Gamo, K., Bencokova, Z., Gastaldo, J., Rénier, W., Chavaudra, N., Favaudon, V., Arlett, C., Foray, N., 2008. DNA double-strand break repair defects in syndromes associated with acute radiation response: at least two different assays to predict intrinsic radiosensitivity? Int. J. Radiat. Biol. 84, 1–19.
Kinner, A., Wu, W., Staudt, C., Iliakis, G., 2008. Gamma-H2AX in recognition and signaling of DNA double-strand breaks in the context of chromatin. Nucleic Acids Res. 36, 5678–5694.
Krueger, S.A., Collis, S.J., Joiner, M.C., Wilson, G.D., Marples, B., 2007. Transition in survival from low-dose hyper-radiosensitivity to increased radioresistance is independent of activation of ATM Ser1981 activity. Int. J. Radiat. Oncol. Biol. Phys. 69, 1262–1271.
Lisby, M., Rothstein, R., 2009. Choreography of recombination proteins during the DNA damage response. DNA Repair (Amst) 8, 1068–1076.
Lisby, M., Barlow, J.H., Burgess, R.C., Rothstein, R., 2004. Choreography of the DNA damage response: spatiotemporal relationships among checkpoint and repair proteins. Cell 118, 699–713.

Lobrich, M., Jeggo, P.A., 2005. The two edges of the ATM sword: co-operation between repair and checkpoint functions. Radiother. Oncol. 76, 112–118.
Maser, R.S., Monsen, K.J., Nelms, B.E., Petrini, J.H., 1997. hMre11 and hRad50 nuclear foci are induced during the normal cellular response to DNA double-strand breaks. Mol. Cell Biol. 17, 6087–6096.
Mirzoeva, O.K., Petrini, J.H., 2001. DNA damage-dependent nuclear dynamics of the Mre11 complex. Mol. Cell Biol. 21, 281–288.
Neumaier, T., Swenson, J., Pham, C., Polyzos, A., Lo, A.T., Yang, P., Dyball, J., Asaithamby, A., Chen, D.J., Bissell, M.J., Thalhammer, S., Costes, S.V., 2012. Evidence for formation of DNA repair centers and dose-response nonlinearity in human cells. Proc. Natl. Acad. Sci. USA 109, 443–448.
Rothkamm, K., Lobrich, M., 2003. Evidence for a lack of DNA double-strand break repair in human cells exposed to very low x-ray doses. Proc. Natl. Acad. Sci. USA 100, 5057–5062.
Rothkamm, K., Kruger, I., Thompson, L.H., Lobrich, M., 2003. Pathways of DNA double-strand break repair during the mammalian cell cycle. Mol. Cell Biol. 23, 5706–5715.
Scully, R., Chen, J., Ochs, R.L., Keegan, K., Hoekstra, M., Feunteun, J., Livingston, D.M., 1997. Dynamic changes of BRCA1 subnuclear location and phosphorylation state are initiated by DNA damage. Cell 90, 425–435.
Stewart, G.S., Wang, B., Bignell, C.R., Taylor, A.M., Elledge, S.J., 2003. MDC1 is a mediator of the mammalian DNA damage checkpoint. Nature 421, 961–966.
Sutherland, J.C., 2006. Repair dependent radiation survival: a stochastic model with Euler gamma function solutions. Phys. Med. Biol. 51, 4883–4901.
Testard, I., Sabatier, L., 1999. Biological dosimetry for astronauts: a real challenge. Mutat. Res. 430, 315–326.
Tsoularis, A., Wallace, J., 2002. Analysis of logistic growth models. Math Biosci. 179, 21–55.
Verhulst, P.-F., 1838. Notice sur la loi que la population suit dans son accroissement. Correspondance mathématique et physique tome II, 3e série, pp. 113–121.
Verhulst, P.-F., 1846. Note sur la loi d'accroisssement de la population. Bulletins de l'Académie Royale des Sciences et Belles Lettres de Bruxelles XIII, 1–3.
Yang, D.Q., Halaby, M.J., Li, Y., Hibma, J.C., Burn, P., 2011. Cytoplasmic ATM protein kinase: an emerging therapeutic target for diabetes, cancer and neuronal degeneration. Drug Discov. Today 16, 332–338.